Appl. Math. Mech. -Engl. Ed., **39**(11), 1605–1616 (2018)

Applied Mathematics and Mechanics (English Edition)

https://doi.org/10.1007/s10483-018-2387-6

Effects of the Reynolds number on a scale-similarity model of Lagrangian velocity correlations in isotropic turbulent flows*

Zhaoyu SHI[1,2], Jincai CHEN[1,3], Guodong JIN[1,2,†]

1. State Key Laboratory of Nonlinear Mechanics (LNM), Institute of Mechanics, Chinese Academy of Sciences, Beijing 100190, China;
2. School of Engineering Science, University of Chinese Academy of Sciences, Beijing 100049, China;
3. School of Engineering, Sun Yat-sen University, Guangzhou 510275, China

(Received Apr. 3, 2018 / Revised May 17, 2018)

Abstract A scale-similarity model of a two-point two-time Lagrangian velocity correlation (LVC) was originally developed for the relative dispersion of tracer particles in isotropic turbulent flows (HE, G. W., JIN, G. D., and ZHAO, X. Scale-similarity model for Lagrangian velocity correlations in isotropic and stationary turbulence. *Physical Review E*, **80**, 066313 (2009)). The model can be expressed as a two-point Eulerian space correlation and the dispersion velocity V. The dispersion velocity denotes the rate at which one moving particle departs from another fixed particle. This paper numerically validates the robustness of the scale-similarity model at high Taylor micro-scale Reynolds numbers up to 373, which are much higher than the original values ($R_\lambda = 66$, 102). The effect of the Reynolds number on the dispersion velocity in the scale-similarity model is carefully investigated. The results show that the scale-similarity model is more accurate at higher Reynolds numbers because the two-point Lagrangian velocity correlations with different initial spatial separations collapse into a universal form compared with a combination of the initial separation and the temporal separation via the dispersion velocity. Moreover, the dispersion velocity V normalized by the Kolmogorov velocity $V_\eta \equiv \eta/\tau_\eta$ in which η and τ_η are the Kolmogorov space and time scales, respectively, scales with the Reynolds number R_λ as $V/V_\eta \propto R_\lambda^{1.39}$ obtained from the numerical data.

Key words turbulent mixing, relative dispersion, Lagrangian velocity correlation, scale-similarity model, dispersion velocity, Reynolds number effect

Chinese Library Classification O357.5
2010 Mathematics Subject Classification 76F05, 82C40

* Citation: SHI, Z. Y., CHEN, J. C., and JIN, G. D. Effects of the Reynolds number on a scale-similarity model of Lagrangian velocity correlations in isotropic turbulent flows. *Applied Mathematics and Mechanics* (*English Edition*), **39**(11), 1605–1616 (2018) https://doi.org/10.1007/s10483-018-2387-6

† Corresponding author, E-mail: gdjin@lnm.imech.ac.cn

Project supported by the Science Challenge Program (No. TZ2016001), the National Natural Science Foundation of China (Nos. 11472277, 11572331, 11232011, and 11772337), the Strategic Priority Research Program, Chinese Academy of Sciences (No. XDB22040104), and the Key Research Program of Frontier Sciences, Chinese Academy of Sciences (No. QYZDJ-SSW-SYS002)

Nomenclature

$\boldsymbol{f}$,	external force;	$\boldsymbol{v}$,	tracer velocity;
$\boldsymbol{k}$,	wavenumber vector;	V,	dispersion velocity;
$k_{\max}$,	maximum wavenumber value;	V_η,	Kolmogorov velocity scale;
$\boldsymbol{r}$,	space separation;	$\boldsymbol{x}_{\rm p}$,	tracer position;
$r_{\rm c}$,	characteristic space scale;	$\boldsymbol{x}_0$,	reference position;
r^*,	rescaled variable;	β,	ratio of Lagrangian to Eulerian integral timescale;
R,	Lagrangian velocity correlation;		
R_λ,	Taylor-scale Reynolds number;	η,	Kolmogorov space scale;
$t_{\rm B}$,	Batchelor time scale;	ν,	kinematic viscosity;
$T_{\rm e}$,	large-eddy turnover time;	τ,	time separation;
t_0,	reference initial time;	$\tau_{\rm c}$,	characteristic time scale;
$\boldsymbol{u}$,	flow field velocity;	τ_η,	Kolmogorov time scale;
U,	sweeping velocity;	$\boldsymbol{\omega}$,	vorticity.
$u_{\rm rms}$,	root mean square of fluctuation velocity;		

1 Introduction

Turbulent flows have the ability to efficiently transport and mix entrained species[1]. The local concentration fluctuation, which determines the chemical reaction rate, is closely related to the relative dispersion of the tracer particles with initially small spatial separations[2–4]. The turbulent dispersion of two or multiple marked tracer particles is typically studied in a Lagrangian reference frame[5]. Taylor[6] expressed a single-particle turbulent dispersion coefficient as the product of the square of the fluid fluctuation velocity and the integral timescale of the one-point Lagrangian velocity correlation (LVC). Batchelor[7–8] investigated a two-particle relative dispersion with initial separations in the inertial subrange by integrating the Lagrangian velocity correlation, and showed that the relative separation at short time exhibited a ballistic regime. Richardson[9] pioneered the investigation of the relative dispersions of particle pairs at large time scales, wherein the initial separations were also in the inertial subrange. The advanced Richardson regime is super diffusive, and is very difficult to be observed in turbulent flows in laboratory[2]. The timescale t_0 corresponding to the initial separation Δ_0, i.e., $t_{\rm B} = (\Delta_0^2/\varepsilon)^{1/3}$, is the transition between the Batchelor regime and the Richardson regime. Thus, the Richardson regime needs a large time separation between the integral timescale and the Kolmogorov timescale as well as a large time separation between the integral timescale and the timescale $t_{\rm B}$ corresponding to the initial separation Δ_0, which leads to the difficulty in obtaining turbulent flows in laboratory with a timescale separation large enough to observe the Richardson regime. Recently, Dhariwal and Bragg[10] studied the particle-pair dispersions with initial spatial separations in the dissipation subrange, and found that the increased separation moments followed an exponential law after extremely long time ($t \gg T_{\rm L}$). The two-point LVC concerning the relative dispersion depends on the instantaneous spatial separations. Thus, the prediction of the relative dispersion relies on the correct modeling for LVCs. Under the "frozen flow" hypothesis, Smith and Hay[11] proposed a model of the LVC expressed by an Eulerian velocity spatial correlation with a linear combination between the spatial and temporal separations. The linear model was a first-order approximation. He et al.[12] further developed a second-order scale-similarity model of the LVC expressed with an Eulerian velocity spatial correlation and a dispersion velocity, and showed that the LVC functions decreased in the spatial and temporal separations. The temporal separation was included in a combined argument into the Eulerian velocity spatial correlation function so as to replace the original spatial separation. The dispersion velocity in the combined argument denotes the separation rate of one particle departing from another fixed particle in the Lagrangian reference frame. He et al.[12] also validated the proposed scale-similarity model of a LVC by using direct numerical simulation (DNS)

data. However, the Reynolds numbers considered in Ref. [12] were very low ($R_\lambda = 66,\ 102$). The scale similarity model should be validated at higher Reynolds number flows with both spatial and temporal separations being located in dissipation and inertial subranges. This is because that the dispersion velocity has different expressions when the spatial and temporal separations are located in different subranges.

From the practical point of view, the integral timescale of the Lagrangian velocity correlation is very important for the closure of particle subgrid scale (SGS) in the large-eddy simulation (LES) of particle-laden turbulent flows[13–14]. The conventional SGS model is usually constructed based on the space-correlation information, and it is shown that the LES based on the convectional SGS model over-predicts the decorrelation scale[15–16]. Yang et al.[17] systematically studied the effects of the SGS model on the relative dispersion of fluid particles, and found that the LES severely under-predicted the relative dispersion and over-predicted the Lagrangian timescales. The under-prediction of relative dispersion existing in LES is also observed in real ocean problems. The same tendency of under-prediction in LES and ocean is due to the low resolution. The small-scale motions dominating the relative dispersion are missed due to the low resolution in LES and the large separation between the drifting instruments used in ocean observation[18].

The objective of this paper is to validate the robustness of the scale similarity model of a LVC at higher Reynolds number flows and to investigate the effects of the Reynolds number on the dispersion velocity, which is a crucial parameter combining the space and time separations in a nonlinear form.

In our study, we will revisit a previous work[12] and utilize the DNS data to study how and to what extent the Reynolds number affects the scale-similarity model. Four Reynolds numbers, i.e.,

$$R_\lambda = 84,\ 107,\ 188,\ 373,$$

are used in the simulations, which correspond to the grid resolutions

$$N^3 = 128^3,\ 256^3,\ 512^3,\ 1\,024^3.$$

We select six LVC curves with different initial space separations for each Reynolds number case, and observe their decorrelation processes. The changes in the dispersion velocity V in the scale-similarity model are emphasized.

The organization of this paper is as follows. Section 2 provides a summary of the governing equations of the fluid phase, the particle tracking method, and relevant simulation parameters. Section 3 gives a concise introduction of the scale-similarity model for LVCs. Section 4 provides the DNS results and discussion, including a rescaled two-point two-time LVC and the variation of the normalized dispersion velocity with different Reynolds numbers. Finally, the conclusions are presented in Section 5.

2 Methodology

In this section, a brief summary of the governing equations for turbulent flows are provided. The turbulent flow field is solved in an Eulerian reference frame, and the trajectories of tracer particles are tracked in a Lagrangian reference frame. The simulation parameters and the used numerical method are also described.

2.1 Fluid phase

Isotropic turbulent flows are simulated in a cubic periodic domain with each side length $L = 2\pi$. The domain is discretized into N^3 grid points, where N is the number of the grid points along one of the three dimensions. The Navier-Stokes (N-S) equations for incompressible

flows are as follows:

$$\frac{\partial \boldsymbol{u}}{\partial t} + \boldsymbol{\omega} \times \boldsymbol{u} + \nabla\Big(\frac{p}{\rho} + \frac{\boldsymbol{u}^2}{2}\Big) = \nu\nabla^2\boldsymbol{u} + \boldsymbol{f}, \tag{1}$$

$$\nabla \cdot \boldsymbol{u} = 0, \tag{2}$$

where $\boldsymbol{u}$ is the fluid velocity, $\boldsymbol{\omega} \equiv \nabla \times \boldsymbol{u}$ is the fluid vorticity, ρ is the fluid density, and ν is the fluid kinematic viscosity. To achieve a stationary turbulent state, we drove the flow by using an external large-scale stochastic force term $\boldsymbol{f}$, which was developed by Eswaran and Pope[19]. We use a dealiased pseudo-spectral method. The maximum wavenumber is

$$k_{\max} = N/3.$$

$\boldsymbol{k} = (k_1, k_2, k_3)$ is the wavenumber vector. The spectral velocity is advanced by using the second-order Adams-Bashforth method. We perform four runs at the Taylor microscale Reynolds numbers $R_\lambda = 84$, 107, 188, and 373. The simulated parameters are shown in Table 1. The flow is driven from $t = 0$ to $t = 3T_\mathrm{e}$, where T_e is the large-scale eddy turnover time, to obtain a steady state. Then, the tracer particles are tracked in the well-developed flow. In our simulations, the spatial resolution is monitored by $k_{\max}\eta$. This value is maintained above 1.0 to ensure the accurate resolutions of the smallest scale motions[20].

Table 1 Flow parameters in the DNS, where $R_\lambda = u_{\mathrm{rms}}^2(15/(\nu\varepsilon))^{1/2}$ is the Taylor microscale Reynolds number, u_{rms} is the root mean square (RMS) velocity, $\eta = (\nu^3/\varepsilon)^{1/4}$ is the Kolmogorov length scale, $T_\mathrm{e} = u_{\mathrm{rms}}^2/\varepsilon$ is the large-scale eddy turnover time, and $\tau_\eta = (\nu/\varepsilon)^{1/2}$ is the Kolmogorov timescale

Simulation grid	128^3	256^3	512^3	$1\,024^3$
R_λ	84	107	188	373
u_{rms}	18.76	18.79	20.01	19.85
η	1.867×10^{-2}	1.365×10^{-2}	5.920×10^{-3}	2.223×10^{-3}
ν	7.500×10^{-2}	4.878×10^{-2}	1.700×10^{-2}	4.500×10^{-3}
τ_η	4.651×10^{-3}	3.819×10^{-3}	2.070×10^{-3}	1.099×10^{-3}
T_e	0.101 4	0.105 6	0.100 5	0.106 0
$k_{\max}\eta$	1.63	1.56	1.67	1.33
Courant-Friedrichs-Lewy (CFL) condition	0.280	0.170	0.260	0.256

2.2 Lagrangian tracking of tracer particles

The equation of motion for a tracer particle is

$$\frac{\mathrm{d}\boldsymbol{x}_\mathrm{p}(t;\boldsymbol{x}_0,t_0)}{\mathrm{d}t} = \boldsymbol{v}(t,\boldsymbol{x}_\mathrm{p};\boldsymbol{x}_0,t_0), \tag{3}$$

where $\boldsymbol{x}_\mathrm{p}(t;\boldsymbol{x}_0,t_0)$ and $\boldsymbol{v}(\boldsymbol{x}_\mathrm{p},t;\boldsymbol{x}_0,t_0)$ are the tracer particle position and velocity, respectively. The particles are seeded in the flow field when the flow is statistically steady. We divide the particles into two sets, which are labeled by odd and even numbers, respectively. A particle pair consists of an odd number particle and an even number particle. We initialize the positions of the odd particles by using pseudo-random numbers denoted as (x_1, y_1, z_1). The positions of the corresponding even particles denoted as (x_2, y_2, z_2) are initialized through the equations as follows:

$$\begin{cases} x_2 = 2\pi x_1 + r_0\cos(2\pi x_1), \\ y_2 = 2\pi y_1 + r_0\sin(2\pi x_1)\cos(2\pi y_1), \\ z_2 = 2\pi z_1 + r_0\sin(2\pi x_1)\sin(2\pi y_1), \end{cases} \tag{4}$$

where r_0 is the given initial separation of a particle pair. The second particle of the particle pair is located on a spherical surface with the radius r_0 relative to the first one. To obtain the Lagrangian velocity $\boldsymbol{u}_{\mathrm{p}}(\boldsymbol{x}_{\mathrm{p}}, t; \boldsymbol{x}_0, t_0)$, we adopt a six-point Lagrangian interpolation from the Eulerian grids to the particle position[20]. Then, we compute the displacement of particles by using a fourth-order Adams-Moulton method[21].

3 Scale similarity model of Lagrangian velocity correlation

A normalized two-point two-time LVC is defined as follows:

$$R(r,\tau) = \frac{\langle \boldsymbol{v}(\boldsymbol{x}_0 + \boldsymbol{r}, t_0 + \tau) \cdot \boldsymbol{v}(\boldsymbol{x}_0, t_0) \rangle}{\langle \boldsymbol{v}(\boldsymbol{x}_0, t_0) \cdot \boldsymbol{v}(\boldsymbol{x}_0, t_0) \rangle}, \tag{5}$$

where the bracket $\langle \cdot \rangle$ denotes the ensemble average conditioned for different particle pairs. $\boldsymbol{v}(\boldsymbol{x}_0, t_0)$ denotes the velocity of a fixed particle at the point $\boldsymbol{x}_0$ at t_0 from an Eulerian viewpoint. $\boldsymbol{v}(\boldsymbol{x}_0 + \boldsymbol{r}, t_0 + \tau)$ denotes the particle velocity at $t_0 + \tau$ passing through the point $\boldsymbol{x}_0 + \boldsymbol{r}$ at the time t_0 from a Lagrangian viewpoint. Therefore, the definition of LVC indeed presents both Lagrangian and Eulerian quantities. $\boldsymbol{r}$ is the spatial separation between the particle pairs, and $r = |\boldsymbol{r}|$. τ denotes a time separation with positive values for forward-in-time dispersions. The two-particle dispersion trajectories are shown in Fig. 1 to visually present the concept of two-point two-time Lagrangian velocity correlations during the pair dispersion of particles. The red and blue particles, marked as A and B, respectively, represent a particle pair, and the black solid line represents their initial space separation $\boldsymbol{r}$. At $t = t_0$, particles A and B are at the positions $\boldsymbol{x}_0$ and $\boldsymbol{x}_0 + \boldsymbol{r}$, respectively. As time advances with the separation τ, the particle positions along their trajectories are denoted as A_n and B_n $(n = 1, 2, 3, \cdots)$ at the time $t = t_0 + \tau_n$. The term $\boldsymbol{v}(\boldsymbol{x}_0 + \boldsymbol{r}, t_0 + \tau) \cdot \boldsymbol{v}(\boldsymbol{x}_0, t_0)$ in Eq. (5) indicates the Lagrangian velocity correlations of particles A and B_n at $t = t_0 + \tau_n$. Equation (5) indicates the average LVCs of all tracked particle pairs, i.e., the ensemble average. The same calculation processes are conducted at other marked time points t_n $(n = 1, 2, 3, \cdots)$.

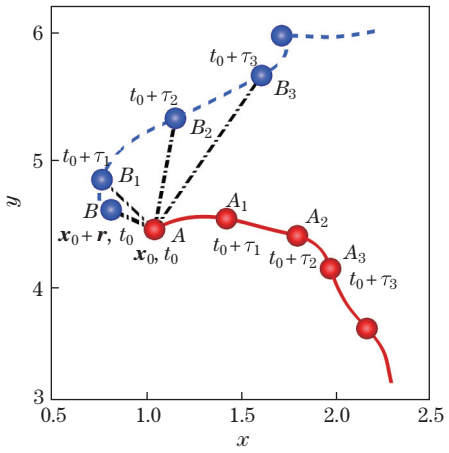

Fig. 1 Trajectories (solid red and dashed blue lines) of a particle pair (red and blue spheres) at different time with a given initial space separation $\boldsymbol{r}$, where the dash-dotted lines link the two particles at two different time to calculate the Lagrangian velocity correlation (color online)

When $\tau = 0$, the LVC $R(r,\tau) = R(r,0)$, and is consistent with a two-point space Eulerian velocity spatial correlation. Under statistically isotropic and stationary assumptions, the

scale-similarity model of LVC is described by a two-point Eulerian velocity correlation and a dispersion velocity V as follows:

$$R(r,\tau) = R(\sqrt{r^2 + V^2\tau^2}, 0), \tag{6}$$

where $V \equiv r_\mathrm{c}/\tau_\mathrm{c}$ and r_c, τ_c are the intersecting points of the contour $R(r,\tau) = C$ in the spatial axis r and the temporal axis τ, respectively. For all points (r,τ) at the same contour level with the crossing points $(0, r_\mathrm{c})$ and $(\tau_\mathrm{c}, 0)$,

$$R(r,\tau) = R(r_\mathrm{c}, 0) = R(0, \tau_\mathrm{c}) = \text{const.} \tag{7}$$

We transform $\sqrt{r^2 + V^2\tau^2}$ as a rescaled variable r^* as follows:

$$R(r,\tau) = R(r^*, 0). \tag{8}$$

The earlier work[12] theoretically derived the dispersion velocity V. The expression of V is given by

$$V^2 = \frac{64}{15}\int_0^\infty E(k)\frac{\sin(kr_\mathrm{c})}{kr_\mathrm{c}}\mathrm{d}k\int_0^k q^2E(q)\mathrm{d}q\Big(\frac{1}{r_\mathrm{c}}\frac{\partial R(r,0)}{\partial r}\Big|_{r=r_\mathrm{c}}\Big)^{-1}, \tag{9}$$

where $E(k)$ is the turbulent energy spectrum, and k is the wave number. From Eq. (9), we observe that the dispersion velocity V is a function of r_c. The spatial intercept length r_c is the corresponding length scale of $R(r,\tau) = \text{const.}$, indicating that the dispersion velocity varies with the space length scale and is a local quantity.

The derivation of the scale-similarity model is considered at the infinite Reynolds numbers. In the DNS flow field with finite Reynolds numbers, the inertial subrange becomes more evident as the Reynolds number increases, which is presented in the time-averaged spectrum for the three runs in Fig. 2. The line with the slope $-5/3$ represents the inertial subrange in the energy spectrum. The relationship of grid nodes and Reynolds number follows $N^3 \propto R_\lambda^{9/2}$ [22], which indicates that the increase in R_λ requires larger grid numbers. A clear $-5/3$ slope in the log-log coordinate is shown in Fig. 2 for the highest Reynolds-numbers at the grid resolution $N^3 = 1\,024^3$, indicating the presence of a well-defined inertial subrange. Additionally, if r_c is in the dissipation subrange and τ_c is in the inertial subrange, the dispersion velocity follows $r_\mathrm{c} \propto \tau_\mathrm{c}^{0.5}$ or $V \propto \tau_\mathrm{c}^{-0.5}$ [12–23], respectively. We also present the Eulerian and Lagrangian second-order structure functions within the dissipation subrange, which are denoted as S_2E and S_2L, respectively. The definition of S_2E and S_2L are expressed as follows:

$$S_\mathrm{2E} = \langle(\boldsymbol{u}(\boldsymbol{x}_0) - \boldsymbol{u}(\boldsymbol{x}_0 + \boldsymbol{r}))^2\rangle, \quad S_\mathrm{2L} = \langle(\boldsymbol{v}(t_0) - \boldsymbol{v}(t_0 + \tau))^2\rangle, \tag{10}$$

where $\boldsymbol{u}$ is the velocity of the Eulerian grid, $\boldsymbol{v}$ is the velocity of the fluid particle. We observe from Fig. 3(a) that the Eulerian structure function S_2E is proportional to r^2 when r is approximately no larger than 5.5η. Figure 3(b) shows that there exists a τ^2 regime for the Lagrangian structure function within $1.2\tau_\eta$, which is consistent with the numerical result of Biferale et al.[24].

4 DNS results

We show the results for the LVC $R(r,\tau)$ at $R_\lambda = 84, 107, 188$, and 373 to investigate how the Reynolds number affects the scale similarity model for LVCs. Figures 4(a) and (b) present 3D contour iso-surfaces and 2D contour iso-lines of two-point two-time Lagrangian velocity correlations at the Reynolds number $R_\lambda = 373$, respectively. As shown in Fig. 4(a), the normalized LVC values reach a peak at the origin point $(r,\tau) = (0,0)$. The correlation values naturally

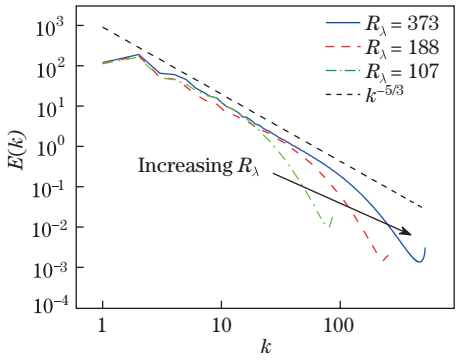

Fig. 2 Energy spectra at different Reynolds numbers, where the dashed line has a slope of $-5/3$, denoting the inertial subrange (color online)

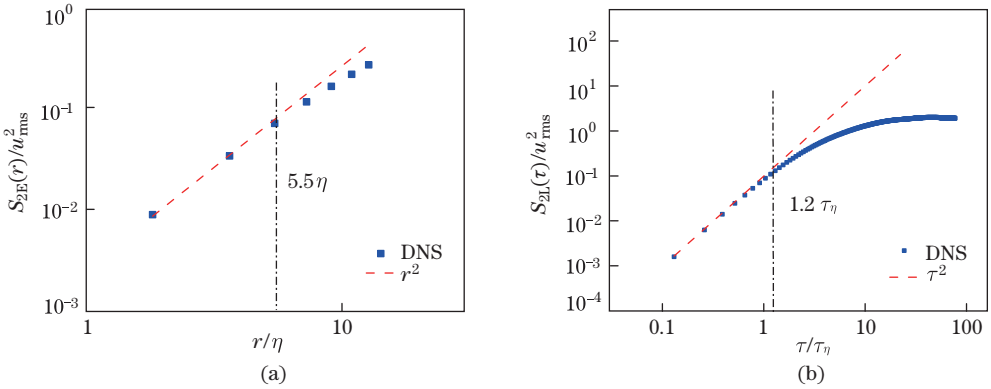

Fig. 3 Eulerian and Lagrangian second-order structure functions at the grid resolution $N^3 = 256^3$ with the normalised space and time separations, respectively (color online)

decrease as the relative separation between the particle pair r and time separation τ increases. From Fig. 4(b), we can observe that the shapes of the contour iso-lines with different values are approximately elliptical. Unlike the Eulerian velocity correlations in the elliptic approximation (EA) model, which are expressed as $R(r,\tau) = R(r^*,0)$ where $r^*=\sqrt{(r-U\tau)^2 + V^2\tau^2}$ and U is the sweeping velocity for shear flows[25–27], there is no preferred direction for the Lagrangian correlation in isotropic turbulence. The principal contours axes are the spatial and temporal axes. The LVC model developed by Smith and Hay, $R(r,\tau) = R(r + U\tau/\beta, 0)$ where β is a constant and is the ratio of the Lagrangian integral timescale to the Eulerian counterpart, is based on the Taylor frozen flow hypothesis without considering the vortex distortion. By contrast, the scale-similarity model is more physical than the Smith-Hay model, which has straight correlation iso-lines. However, these straight lines are not true because the values of the Lagrangian velocity correlation along a straight contour line at two different time and space separations cannot be the same. We plot the profiles of Fig. 4(a) at $\tau = 0$ and $r = 0$ in Figs. 5(a) and 5(b), respectively, to show the changes in the Lagrangian velocity correlation along the spatial and temporal directions.

The left panel of Fig. 6 presents the R versus τ curves at four Reynolds numbers. The correlation curves with six different initial spatial separations denoted as r_0 are initially separated. However, when they are plotted as a function of the combined separation $r^* = \sqrt{r^2 + (V\tau)^2}$ in the right panel of Fig. 6, the correlation curves are collapsed into a single curve, as expected

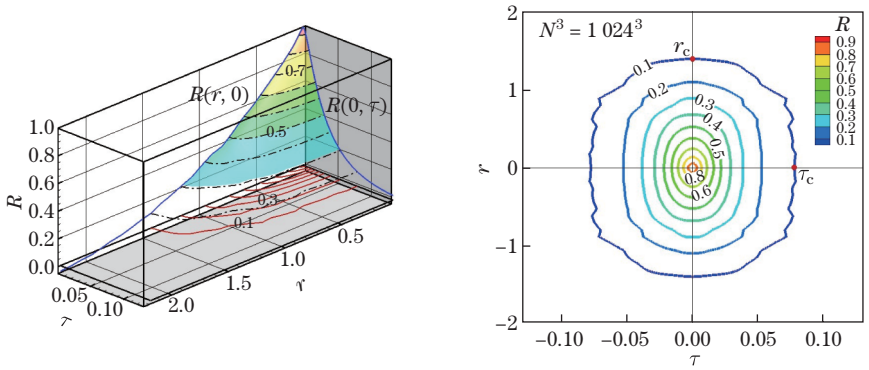

(a) Contour surface (b) Isocorrelation contour lines

Fig. 4 Contour surface of the LVC plotted against the space and time separations and the isocorrelation contour lines at the grid resolution $N^3 = 1\,024^3$ (color online)

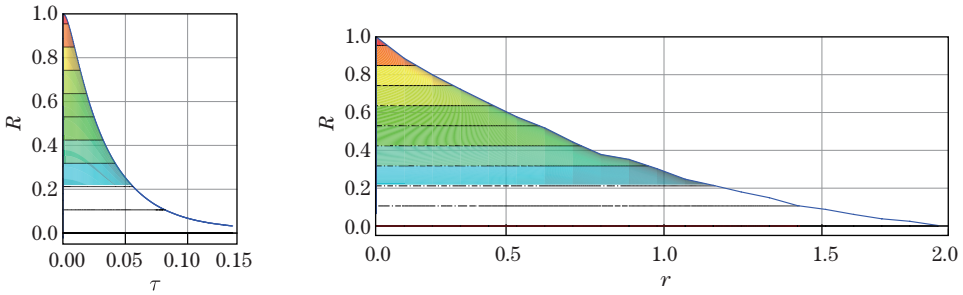

(a) Temporal separation (b) Spatial separation

Fig. 5 Lagrangian velocity correlation curves plotted against the temporal separation τ and the spatial separation r, where the R versus τ curves correspond to the profiles at $\boldsymbol{r} = 0$, and the R versus r curves correspond to the profiles at $\tau = 0$ (color online)

according to $R(r, \tau) = R(r^*, 0)$. As observed in Fig. 6, the correlation curves R versus r^* and R versus τ present similar decorrelation processes at four Reynolds numbers. These four cases validate the scale-similarity model for a wide range of Reynolds numbers. It is expected that the dispersion velocity increases with increasing the Reynolds number when the initial separations of particle pairs are within the dissipation scale because the flow becomes more energetic and intermittent at small scales when the Reynolds number increases.

We next address the dispersion velocity V, which represents the aspect ratio of the maximum intercept length to the minimum intercept length. The horizontal and vertical axes in Fig. 7 represent the lengths of the minor (temporal) and major (spatial) axes of the isocorrelation contours obtained from the DNS data, respectively. Two different scaling ranges exist. One follows $r_c \propto \tau_c$ with a constant V, and the other follows $r_c \propto \tau_c^{0.5}$, i.e.,

$$V \propto \tau_c^{-0.5}.$$

From the figure, we can see that the linear time scale range increases as the Reynolds number increases. Moreover, we compare the normalized r_c versus τ_c at four Reynolds numbers in Fig. 8. The normalized relative separation r_c is larger at higher Reynolds numbers at the same normalized time τ_c. We study the dispersion velocity V over a constant linear range. Figure 9 presents the normalized dispersion velocity V as a function of the Reynolds number R_λ. In the linear range, the dispersion velocity increases as R_λ increases, following a power law $V/V_\eta \propto R_\lambda^{1.39}$,

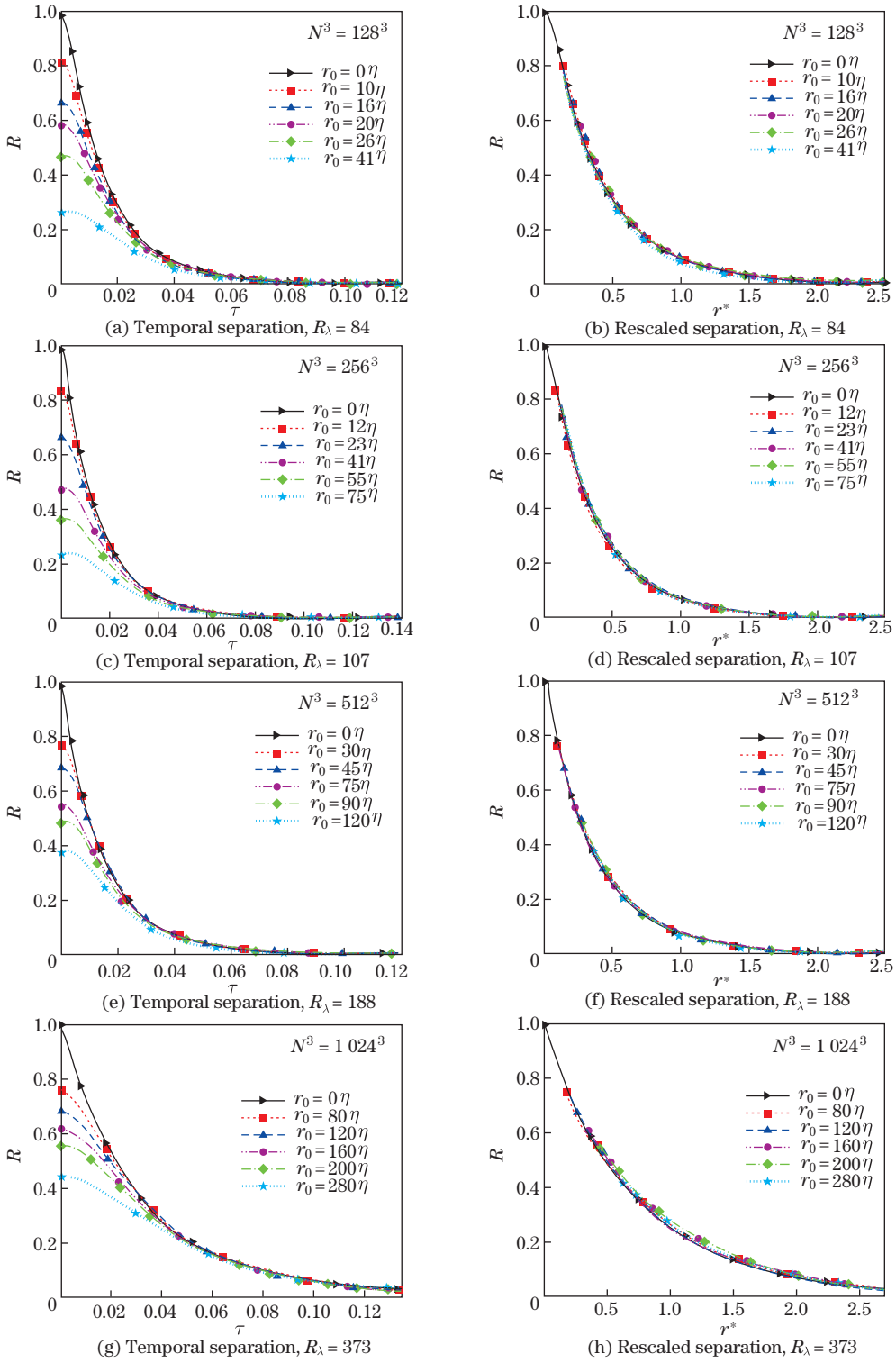

Fig. 6 LVCs against the temporal separation and rescaled separation with different r_0 (color online)

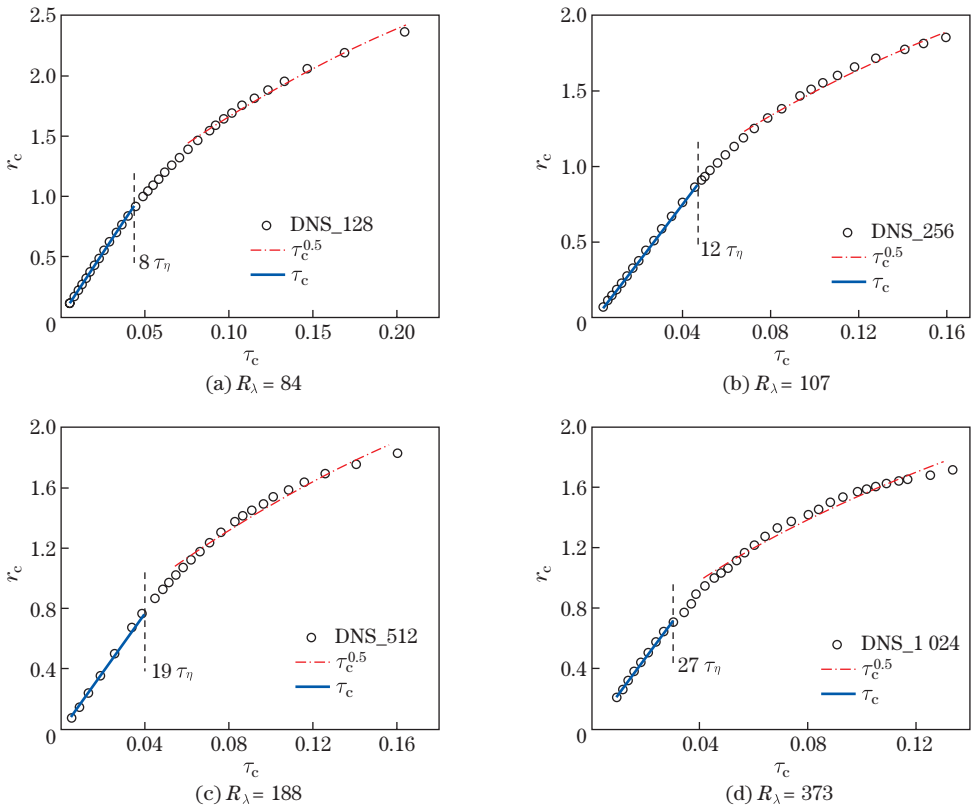

Fig. 7 Intercept lengths of the spatial axes r_c of the isocorrelation contours versus the intercept lengths of the temporal axes τ_c at four grid resolutions (color online)

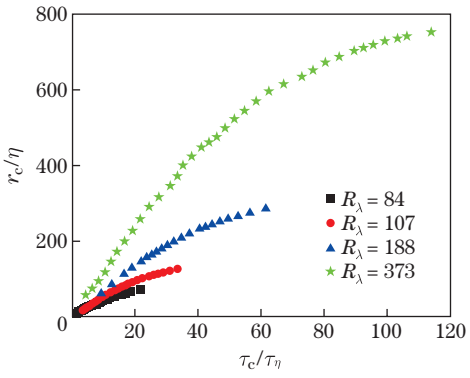

Fig. 8 Normalized intercept lengths of the spatial axes of the isocorrelation contour plotted against the normalized intercept lengths of the temporal axes at different R_λ (color online)

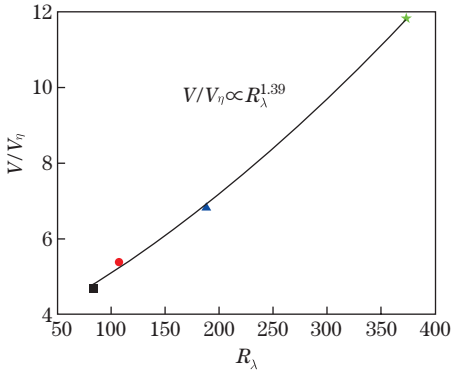

Fig. 9 Normalized dispersion velocity V of dissipation scale as a function of R_λ

wherein $V_\eta = \eta/\tau_\eta$. From the above analysis, we conclude that the Reynolds number affects the dispersion velocity values, and the scale-similarity model of the LVC remains valid for different Reynolds numbers.

5 Conclusions

In this paper, we validate the following scale similarity model for the LVC

$$R(r,\tau) = R(\sqrt{r^2 + (V\tau)^2}, 0)$$

at $R_\lambda = 84, 107, 188$, and 373 by using DNS. From the simulation results, the main characteristics of the scale-similarity model, including the elliptic approximation in the shape of the LVC and the scaling laws of the dispersion velocity, exhibit high consistency at different Reynolds numbers. The LVC curves with different initial space separations, as a function of the rescaled separation $r^* = \sqrt{r^2 + (V\tau)^2}$, collapse into a single curve at the simulated Reynolds numbers. However, the dispersion velocities V at the temporal dissipation scale are influenced by the Reynolds number. First, the linear range increases when the Reynolds number increases. Second, the normalized value of V at the dissipation scale increases as the Reynolds number increases. The scaling law is presented as $V/V_\eta \propto R_\lambda^{1.39}$. Due to the increased dispersion velocity, the two-particle relative separation is faster at higher Reynolds numbers.

References

[1] DIMOTAKIS, P. E. Turbulent mixing. *Annual Review of Fluid Mechanics*, **37**, 329–356 (2006)

[2] BOURGOIN, M., OUELLETTE, N. T., XU, H. T., BERG, J., and BODENSCHATZ, E. The role of pair dispersion in turbulent flow. *Science*, **311**, 835–838 (2005)

[3] SAWFORD, B. Turbulent relative dispersion. *Annual Review of Fluid Mechanics*, **33**, 289–317 (2001)

[4] SALAZAR, J. P. L. C. and COLLINS, L. R. Two-particle dispersion in isotropic turbulent flows. *Annual Review of Fluid Mechanics*, **41**, 405–432 (2009)

[5] TOSCHI, F. and BODENSCHATZ, E. Lagrangian properties of particles in turbulence. *Annual Review of Fluid Mechanics*, **41**, 375–404 (2009)

[6] TAYLOR, G. Diffusion by continuous movements. *Proceedings of the London Mathematical Society*, **s2-20**, 196–212 (1922)

[7] BATCHELOR, G. K. The application of the similarity theory of turbulence to atmospheric diffusion. *Quarterly Journal of the Royal Meteorological Society*, **76**, 133–146 (1950)

[8] BATCHELOR, G. K. Diffusion in a field of homogeneous turbulence: II. The relative motion of particles. *Mathematical Proceedings of the Cambridge Philosophical Society*, **48**, 345–362 (1952)

[9] RICHARDSON, L. F. Atmospheric diffusion shown on a distance-neighbour graph. *Proceedings of the Royal Society A*, **110**, 709–737 (1926)

[10] DHARIWAL, R. and BRAGG, A. Tracer particles only separate exponentially in the dissipation range of turbulence after extremely long times. *Physical Review Fluids*, **3**, 034604 (2018)

[11] SMITH, F. and HAY, J. The expansion of clusters of particles in the atmosphere. *Quarterly Journal of the Royal Meteorological Society*, **87**, 82–101 (1961)

[12] HE, G. W., JIN, G. D., and ZHAO, X. Scale-similarity model for Lagrangian velocity correlations in isotropic and stationary turbulence. *Physical Review E*, **80**, 066313 (2009)

[13] JIN, G. D., HE, G. W., and WANG, L. P. Large-eddy simulation of turbulent collision of heavy particles in isotropic turbulence. *Physics of Fluids*, **22**, 055106 (2010)

[14] JIN, G. D. and HE, G. W. A nonlinear model for the subgrid timescale experienced by heavy particles in large eddy simulation of isotropic turbulence with a stochastic differential equation. *New Journal of Physics*, **15**, 035011 (2013)

[15] HE, G. W., WANG, M., and LELE, S. K. On the computation of space-time correlations by large-eddy simulation. *Physics of Fluids*, **16**, 3859–3867 (2004)

[16] HE, G. W., RUBINSTEIN, R., and WANG, L. P. Effects of subgrid-scale modeling on time correlations in large eddy simulation. *Physics of Fluids*, **14**, 2186–2193 (2002)

[17] YANG, Y., HE, G. W., and WANG, L. P. Effects of subgrid-scale modeling on Lagrangian statistics in large-eddy simulation. *Journal of Turbulence*, **9**, 1–24 (2008)

[18] POJE, A. C., OZGÖKMEN, T. M., LIPPHARDT, B. L., JR, HAUS, B. K., RYAN, E. H., HAZA, A. C., JACOBS, G. A., RENIERS, A. J., OLASCOAGA, M. J., NOVELLI, G., GRIFFA, A., BERON-VERA, F. J., CHEN, S. S., COELHO, E., HOGAN, P. J., KIRWAN, A. D., JR, HUNTLEY, H. S., and MARIANO, A. J. Submesoscale dispersion in the vicinity of the deepwater horizon spill. *Proceedings of the National Academy of Sciences of the United States of America*, **111**, 12693–12698 (2014)

[19] ESWARAN, V. and POPE, S. B. An examination of forcing in direct numerical simulations of turbulence. *Computers and Fluidse*, **16**, 257–278 (1988)

[20] YEUNG, P. K. and POPE, S. B. Lagrangian statistics from direct numerical simulations of isotropic turbulence. *Journal of Fluid Mechanics*, **207**, 531–586 (1989)

[21] PRESS, W. H., TEUKOLSKY, S. A., VETTERLING, W. T., and FLANNERY, B. *Numerical Recipes in Fortran*: *the Art of Scientific Computing*, Cambridge University Press, New York (1993)

[22] POPE, S. B. *Turbulent Flows*, Cambridge University Press, Cambridge (2000)

[23] MONIN, A. S. and YAGLOM, A. M. *Statistical Fluid Mechanics*: *Mechanics of Turbulence*, MIT Press, Cambridge (1975)

[24] BIFERALE, L. Lagrangian structure functions in turbulence: experimental and numerical results. *Physics of Fluids*, **20**, 065103 (2008)